Hindawi
Journal of Mathematics
Volume 2023, Article ID 2323418, 12 pages
https://doi.org/10.1155/2023/2323418

Research Article

Adaptive Hierarchical Collocation Method for Solving Fractional Population Diffusion Model

Linqiang Yang,[1] Yafei Liu,[1] Hongmei Ma,[2] Xue Liu,[1] and Shuli Mei[1]

[1]*College of Information and Electrical Engineering, China Agricultural University, Beijing 100083, China*
[2]*Yantai Research Institute, China Agricultural University, Yantai 264000, China*

Correspondence should be addressed to Shuli Mei; meishuli@cau.edu.cn

Received 25 April 2023; Revised 26 June 2023; Accepted 7 July 2023; Published 7 September 2023

Academic Editor: J. F. Gómez-Aguilar

The fractional population diffusion model is crucial for pest prevention. This paper presents an adaptive hierarchical collocation method for solving this model, enhancing the efficiency of algorithms based on Low-Complexity Shannon-Cosine wavelet derived from combinatorial identity theory. This function, an improvement over previous constructs, mitigates the need for iterative computation of parameters and boasts advantages like interpolation, symmetry, and compact support. The method's extension to other time-fractional partial differential equations (PDEs) is also possible. The algorithm's complexity analysis illustrates the concise function's efficiency advantage over the original expression when solving time-fractional PDEs. Comparatively, the method exhibits superior numerical performance to alternative wavelet spectral methods like the Shannon–Gabor wavelet.

1. Introduction

Fisher, in his 1937 article, "The wave of advance of advantageous genes," proposed the population diffusion model, which is utilized in population dynamics to describe the spatial spread of an advantageous allele, and explored its traveling wave solutions [1]. In recent years, the population diffusion model has found broad applications in numerous fields such as epidemics [2], population growth prediction, and propagation of invasive species [3], among others. While the population diffusion model falls under the category of reaction-diffusion equations, obtaining its analytical solution remains challenging despite it being one of the simplest nonlinear reaction-diffusion equations.

In the case of the population diffusion model, many different numerical methods have been proposed to approximate the solution, such as the homotopy perturbation method (HPM) [4] and the residual power series method (RPSM) [5]. Compared with the above methods, the spectral method [6] offers higher accuracy but lower efficiency. Wavelet analysis [7], which has emerged since the mid-80s, serves as a set of mathematical tools to solve a variety of problems in signal and image analysis [2, 8]. As an efficient and effective tool, wavelets [9] have been widely used in many areas, playing a crucial role, especially in signal analysis.

The Shannon wavelet [10] possesses many excellent numerical properties, such as orthogonality, interpolation, smoothness, vanishing moments, and symmetry, but lacks compact support. The property of compact support is useful in improving numerical precision and efficiency. To overcome the shortcoming of the Shannon wavelet function, Mei and Gao [11] constructed the Shannon-Cosine wavelet. It acts as a real wavelet function that retains most of the excellent properties of the Shannon wavelet. Moreover, the proposed wavelet function overcomes the shortcoming of the common windowed or truncated Sinc function, that is, the approximation error does not vanish as the sampling step tends to zero.

The Shannon-Cosine wavelet, widely used in various fields such as image denoising [8, 12], inpainting [13], geometry modeling [14], signal processing [15], option pricing [16], computational mathematics, and control engineering [14], includes a trigonometric series. Interval theory has excellent versatility in describing imprecise data. The theory has been continuously improved and developed, and it has

now become an active branch in the field of computational mathematics. Combining interval theory with wavelet function optimization can effectively improve wavelet performance. Mei et al. [17] proposed an interval wavelet construction method with interpolation properties based on the generalized variational principle.

More specifically, the constructed wavelet contains the trigonometric series; however, the coefficients of the cosine function need to be calculated in advance, and there is indeed a possibility to avoid the calculation of coefficients. To overcome this shortcoming, Low-Complexity Shannon-Cosine wavelet is proposed, and it has been proved that the Low-Complexity Shannon-Cosine wavelet is equivalent to the Shannon-Cosine wavelet of trigonometric series by using the relevant properties of combinatorial numbers. As a result, the number of types of parameters in the Shannon-Cosine wavelet function is successfully reduced.

To make the distinction clear, our convention is to use italic fonts for scalar functions, roman fonts for vector functions, and bold roman fonts for matrix functions. We thus follow the notation described below:

$$\begin{aligned} \text{scalar: } H(z) &= \sum_n h_n z^n, \\ \text{vector: } H(z) &= \sum_n h_n z^n, \\ \textbf{matrix: } \mathbf{H}(z) &= \sum_n \mathbf{h}_n z^n. \end{aligned} \tag{1}$$

The rest of the article is organized as follows. The Shannon-Cosine wavelet and Low-Complexity Shannon-Cosine wavelet are introduced in Section 2, and the properties of the Low-Complexity Shannon-Cosine wavelet and the proof process, demonstrating that it is essentially equivalent to the Shannon-Cosine wavelet in the trigonometric series, are given in Section 3. In Section 4, numerical results are provided. Finally, Section 5 focuses on the conclusions.

2. Definitions of the Shannon-Cosine Wavelet and Low-Complexity Shannon-Cosine Wavelet

Mei and Gao [11] successfully constructed the Shannon-Cosine wavelet by applying the windowed function to the Shannon wavelet. The Shannon-Cosine kernel function is a real wavelet function, which differs from the Shannon–Gabor wavelet that can only be regarded as a quasi-wavelet.

This kernel function is a compactly supported function that preserves the interpolation property and satisfies the wavelet normalization requirement. It overcomes the limitations of other functions like the Shannon–Gabor wavelet and truncated Sinc functions, specifically the nonvanishing reconstruction error as sampling approaches zero. Offering high precision and efficiency, the Shannon-Cosine function is particularly effective for solving various partial differential equations and can be generalized for multiscale cases.

The Shannon-Cosine scale function S_O is composed of three parts: the Sinc function, the weighting function, and the Heaviside function, which is defined as follows:

$$\begin{aligned} S_O(x) &= \frac{\sin(\pi x)}{\pi x} T_O^m(x) R_N(x), \\ T_O^m(x) &= \sum_{n=0}^{m} a_n \cos\left(\frac{2n\pi x}{N}\right), \end{aligned} \tag{2}$$

where

$$\begin{aligned} a_n &= \frac{(-1)^n \prod_{i=1}^{n-1} i^2 a_0 - \sum_{k=n+1}^{m} (-1)^k \prod_{j=1}^{n-1} \left(k^2 - j^2\right) a_k}{(-1)^n \prod_{t=1}^{n-1} \left(n^2 - t^2\right)}, \\ \sum_{n=0}^{m} a_n &= 1, \end{aligned} \tag{3}$$

and $R_N(x) = \chi(x + N/2) - \chi(x - N/2)$, N is a constant that satisfies $\int_{-\infty}^{+\infty} S_O(x) = 1$, the value of N is not unique, and $\chi(x)$ is the Heaviside function, which is defined as follows:

$$\chi(x) = \begin{cases} 0, & x < 0, \\ \dfrac{1}{2}, & x = 0, \\ 1, & x > 0. \end{cases} \tag{4}$$

The contrasts between functions $S_O(x)$ and $Sinc(x)$ are illustrated in Figure 1. When compared to $\mathrm{Sinc}(x)$, $S_O(x)$ demonstrates the compact support property and adheres to the partition of unity.

The simplified Shannon-Cosine scale function $S_N(x)$ is obtained by modifying the original Shannon-Cosine scale function, specifically by raising the cosine function to a positive even power number. This modification highlights the scale's dependence on cosine similarity and results in a more streamlined function, i.e.,

$$\begin{aligned} S_N(x) &= \frac{\sin(\pi x)}{\pi x} T_N^m(x) R_N(x), \\ T_N^m(x) &= \cos^{2m}\left(\frac{\pi x}{N}\right). \end{aligned} \tag{5}$$

To facilitate differentiation from the simplified form of the Shannon-Cosine wavelet below, the Shannon-Cosine wavelet [11] and the simplified Shannon-Cosine wavelet are denoted as S_O and S_N. The difference between the two forms of the Shannon-Cosine wavelet function is just the difference between T_N^m and T_O^m. T_N^m is a power function with respect to $\cos(\pi x/N)$. So, the time complexity of T_N^m is $O(\log m)$. For the original Shannon-Cosine wavelet

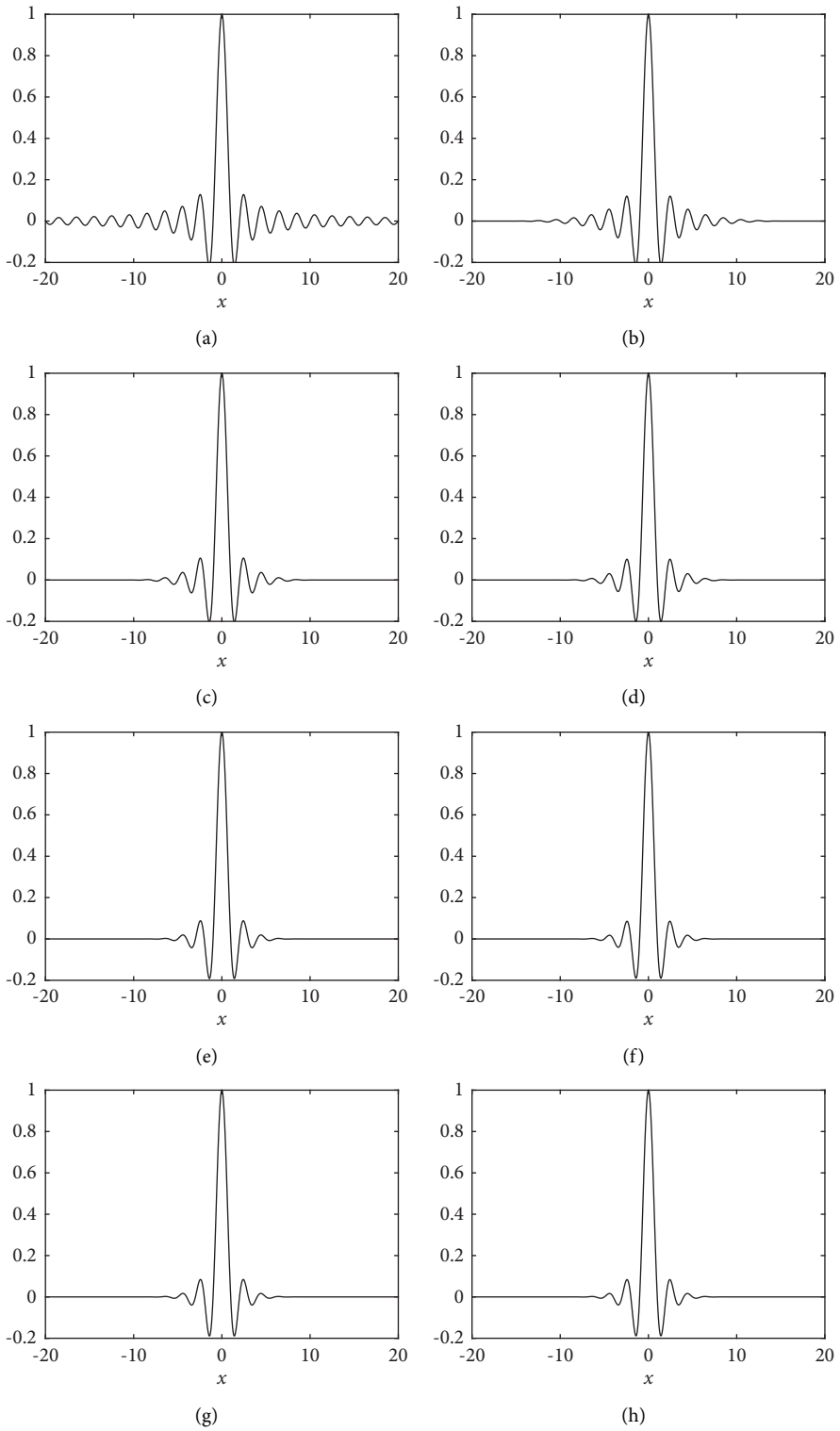

Figure 1: Comparison between $\mathrm{Sinc}(x)$ and Shannon-Cosine scaling function $S_O(x)$. (a) Shannon scaling function. (b) Shannon-Cosine scaling function $m = 1$. (c) Shannon-Cosine scaling function $m = 2$. (d) Shannon-Cosine scaling function $m = 3$. (e) Shannon-Cosine scaling function $m = 4$. (f) Shannon-Cosine scaling function $m = 5$. (g) Shannon-Cosine scaling function $m = 6$. (h) Shannon-Cosine scaling function $m = 7$.

function, the corresponding T_O^m expressed in equation (2) can be rewritten as follows. For convenience, let $\alpha = \pi x/N$; then,

$$\begin{aligned} T_O^m(x) &= \sum_{n=0}^{m} a_n \cos(2n\alpha) \\ &= a_0 + a_1\cos(2\alpha) + a_2\cos(4\alpha) \\ &\quad + a_3\cos(6\alpha) + \cdots + a_n\cos(2n\alpha) \\ &\quad + \cdots + a_m\cos(2m\alpha). \end{aligned} \tag{6}$$

To improve the numerical efficiency, $\cos(2n\alpha)$ can be calculated employing the recurrence formula as follows:

$$\begin{aligned} \cos(2\alpha) &= 2\cos^2(\alpha) - 1, \\ \sin(2\alpha) &= \sqrt{1-\cos^2(2\alpha)}, \\ \cos(4\alpha) &= \cos^2(\alpha) - \sin^2(\alpha), \\ \sin(4\alpha) &= 2\sin(2\alpha)\cos(2\alpha), \\ \cos(6\alpha) &= \cos(4\alpha + 2\alpha) \\ &= \cos(4\alpha)\cos(2\alpha) - \sin(4\alpha)\sin(2\alpha), \\ \sin(6\alpha) &= \sin(4\alpha + 2\alpha) \\ &= \sin(4\alpha)\cos(2\alpha) + \cos(4\alpha)\sin(2\alpha), \\ &\vdots \\ \cos(2n\alpha) &= \cos((2n-1)\alpha + 2\alpha) \\ &= \cos((2n-1)\alpha)\cos(2\alpha) \\ &\quad - \sin((2n-1)\alpha)\sin(2\alpha), \\ \sin(2n\alpha) &= \sin((2n-1)\alpha + 2\alpha) \\ &= \sin((2n-1)\alpha)\cos(2\alpha) \\ &\quad + \cos((2n-1)\alpha)\sin(2\alpha), \\ &\vdots \\ \cos(2m\alpha) &= \cos((2m-1)\alpha + 2\alpha) \\ &= \cos((2m-1)\alpha)\cos(2\alpha) \\ &\quad - \sin((2m-1)\alpha)\sin(2\alpha), \\ \sin(2m\alpha) &= \sin((2m-1)\alpha + 2\alpha) \\ &= \sin((2m-1)\alpha)\cos(2\alpha) \\ &\quad + \cos((2m-1)\alpha)\sin(2\alpha). \end{aligned} \tag{7}$$

Therefore, the time complexity of the original Shannon-Cosine wavelet function is $5m$, that is, $O(m)$ in big O notation. It is straightforward to see that the time complexity of the new form of the Shannon-Cosine wavelet is much lower than that of the original format. This is the reason why we propose a new form of the Shannon-Cosine wavelet in this research.

To more clearly demonstrate the advantages of the constructed wavelet, the simplified Shannon-Cosine wavelet is renamed as the Low-Complexity Shannon-Cosine wavelet.

$$\begin{aligned} T_O^0(x) &= T_N^0(x) = \cos\left(\frac{0\pi x}{N}\right), \\ T_O^1(x) &= T_N^1(x) = \frac{1}{2}\cos\left(\frac{0\pi x}{N}\right) + \frac{1}{2}\cos\left(\frac{2\pi x}{N}\right), \\ T_O^2(x) &= T_N^2(x) = \frac{3}{8}\cos\left(\frac{0\pi x}{N}\right) + \frac{1}{2}\cos\left(\frac{2\pi x}{N}\right) \\ &\quad + \frac{1}{8}\cos\left(\frac{4\pi x}{N}\right). \end{aligned} \tag{8}$$

Indeed, it is easy to see that $T_N^m = T_O^m$ does hold for some not too large m, which seems to imply

$$\forall m \in \mathbb{Z}^+, T_N^m(x) \equiv T_O^m(x). \tag{9}$$

3. Equivalence Proof of Two Forms of Shannon-Cosine Wavelets

The differences between the two forms of Shannon-Cosine wavelet mainly appear in the window function, that is, $T_N^m(x)$ and $T_O^m(x)$, the latter is a trigonometric series, and the former is a positive even power of the cosine function.

In this section, it will be proved that the two forms of the Shannon-Cosine wavelet are equivalent, and the Low-Complexity form possesses smaller time complexity than the original form.

The relevant properties of combinatorial numbers $C_m^n = m!/(n!(m-n)!)$ are introduced in reference [18], the difference method is an effective method for proving certain combinatorial constants. The difference operator of an arbitrary function $f(x)$ is defined as $\Delta f(x) = f(x+1) - f(x)$, which is called the value of the first-order difference of f at x.

The multiorder difference operator deduced from the first-order difference operator is $\Delta^2 f(x) = \Delta(\Delta f(x))$, $\Delta^n f(x) = \Delta(\Delta^{n-1} f(x))$.

The other two operators also need to be introduced in this paper, one for the constant operator $If(x) = f(x)$ and the other for the displacement operator $Ef(x) = f(x+1)$.

It is easy to know the following formula, $E^n f(x) = f(x+n)$ and $I^n f(x) = f(x)$, so $\Delta f(x) = Ef(x) - If(x) = (E-I)f(x)$.

In other words, $\Delta = E - I$, from which we obtain

$$\begin{aligned} \Delta^n &= (E-I)^n \\ &= \sum_{k=0}^{n} C_n^k (-I)^k E^{n-k} \\ &= \sum_{k=0}^{n} (-1)^k C_n^k I^k E^{n-k} \\ &= \sum_{k=0}^{n} (-1)^{n-k} C_n^k E^k I^{n-k}. \end{aligned} \tag{10}$$

Lemma 1. *Let $f(x)$ be any function; then,*

$$\begin{aligned}\Delta^n f(x) &= \sum_{k=0}^{n} (-1)^k C_n^k f(x+n-k) \\ &= \sum_{k=0}^{n} (-1)^{n-k} C_n^k f(x+k).\end{aligned} \tag{11}$$

Proof. By using two different representations Δ^n, the following equation holds:

$$\begin{aligned}\Delta^n f(x) &= \left(\sum_{k=0}^{n} (-1)^k C_n^k E^{n-k} I^k\right) f(x) \\ &= \sum_{k=0}^{n} (-1)^k C_n^k E^{n-k} I^k f(x) \\ &= \sum_{k=0}^{n} (-1)^k C_n^k E^{n-k} f(x) \\ &= \sum_{k=0}^{n} (-1)^k C_n^k f(x+n-k), \\ \Delta^n f(x) &= \left(\sum_{k=0}^{n} (-1)^{n-k} C_n^k E^k I^{n-k}\right) f(x) \\ &= \sum_{k=0}^{n} (-1)^{n-k} C_n^k E^k I^{n-k} f(x) \\ &= \sum_{k=0}^{n} (-1)^{n-k} C_n^k E^{n-k} f(x) \\ &= \sum_{k=0}^{n} (-1)^{n-k} C_n^k f(x+k).\end{aligned} \tag{12}$$

Let $\{a_n\}$ be a series; if its p-order difference series $\{\Delta^p a_n\}$ is not a zero series and its $p+1$-order difference series $\{\Delta^{p+1} a_n\}$ is a zero series, then $\{a_n\}$ is said to be a p-order equivariant series. □

Lemma 2. *If $P(x) = \sum_{k=0}^{p} a_k x^{p-k}$ is a p-order polynomial, then the series $\{P(n)\}$ is an equivariant series of the order p.*

Proof

$$\begin{aligned}\Delta^p P(n) &= \Delta^p \left(\sum_{k=0}^{p} a_k x^{p-k}\right) \\ &= \sum_{k=0}^{p} a_k \Delta^p x^{p-k} \\ &= a_0 p!,\end{aligned} \tag{13}$$

and $\Delta^{p+1} P(n) = 0$.

Thus, the series $\{P(n)\}$ is an equivariant series of p order. □

Lemma 3. *If a $\{a_k\}$ is an equivariant series of order p and $n > p$, then*

$$\sum_{k=0}^{n} (-1)^k a_k C_n^k = 0. \tag{14}$$

Proof. From Lemmas 1 and 2, it can be derived that $\sum_{k=0}^{n} (-1)^k C_n^k a_k = (-1)^n \Delta^n a_0 = 0$. □

Lemma 4. *If $P(x) = a_0 x^p + a_1 x^{p-1} + \cdots + a_p$ is a polynomial of order p and $n > p$, then $\sum_{k=0}^{n} (-1)^k P(k) C_n^k = 0$.*

Proof. Assuming that $P(k)$ is a polynomial of order p, we can conclude from Lemma 2 that $P(k)$ is an equivariant series of order p, and the conclusion above holds based on Lemma 3. □

Theorem 5. *The original Shannon-Cosine scale function $S_O(x)$ and the Low-Complexity scale function $S_N(x)$ are equivalent, i.e., $\forall m \in \mathbb{Z}^+, S_O(x) \equiv S_N(x)$.*

Proof. Let $\mathrm{B} = (1, 0, \ldots, 0)^T$ and

$$M = \left[M_0, M_1, M_2, M_3, \ldots, M_r, \ldots, M_m\right]^T. \tag{15}$$

The column vector consisting of the coefficients a_i of $T_O^m(x)$ in the scale function $S_O(x)$ satisfies the equation [11]

$$\mathrm{MX} = B. \tag{16}$$

When $= 1, 2, 3$, $\det(M) = -2, -8, 384 \neq 0$.

When $m > 3$, some mathematical notations are defined in advance:

$$\begin{aligned}Z_m^n &\coloneqq \{1 \le i < j \le m, i, j \in Z \backslash n\}, \\ V_m^n &\coloneqq \prod_{i,j \in Z_m^n} \left(j^2 - i^2\right), \quad n = 0, 1, 2, \ldots, m.\end{aligned} \tag{17}$$

Expand the determinant $\det(M)$ by the first row according to the rules for calculating determinants.

If m is an arbitrary even number and > 2, the value of the determinant of the matrix M is

$$\begin{aligned}\det(M) &= (-1)^{m/2} V_m^0 + \sum_{j=1}^{m} (-1)^j (-1)^{m/2-j} \frac{(m!)^2}{j^2} V_m^j \\ &= (-1)^{m/2} \left(V_m^0 + \sum_{j=1}^{m} \frac{(m!)^2}{j^2} V_m^j\right).\end{aligned} \tag{18}$$

If m is an arbitrary odd number and > 1, the value of the determinant of the matrix M is

$$\begin{aligned}\det(M) &= (-1)^{m+1/2} V_m^0 \\ &\quad + \sum_{j=1}^{m} (-1)^j (-1)^{m+1/2-j} \frac{(m!)^2}{j^2} V_m^j \\ &= (-1)^{m+1/2} \left(V_m^0 + \sum_{j=1}^{m} \frac{(m!)^2}{j^2} V_m^j\right).\end{aligned} \tag{19}$$

Because $V_m^n > 0, n = 0, 1, \cdots, \forall m > 0, \det(M) \neq 0$ and the rank of the matrix M is $m + 1$ and the equation $MX = B$ has a unique solution.

Regarding the expansion of the high power of the cosine function, there is a conclusion that holds $2^n \cos^n(x) = \sum_{k=0}^{n} C_n^k \cos(n - 2k)x$, and let $c_0 = 2^{-2m} C_{2m}^m, c_k = 2^{1-2m} C_{2m}^{m-k}$, $k = 1, \cdots m$, so

$$\begin{aligned} T_N^m(x) &= \cos^{2m}\left(\frac{\pi x}{N}\right) \\ &= 2^{-2m} \sum_{k=0}^{2m} C_{2m}^k \cos(2m - 2k)\frac{\pi x}{N} \\ &= 2^{-2m} C_{2m}^{m-n} \cos\left(\frac{0\pi x}{N}\right) \\ &\quad + \sum_{n=1}^{m} 2^{1-2m} C_{2m}^{m-n} \cos\left(\frac{2n\pi x}{N}\right) \\ &= \sum_{n=0}^{m} c_n \cos\left(\frac{2n\pi x}{N}\right). \end{aligned} \tag{20}$$

Consider the first row of the matrix:

$$\begin{aligned} M_0 C &= \sum_{k=0}^{m} c_k = c_0 + \sum_{k=1}^{m} c_k \\ &= 2^{-2m}\left(C_{2m}^m + \sum_{k=1}^{m} 2C_{2m}^{m-k}\right) \\ &= 2^{-2m}\left(C_{2m}^m + \sum_{k=1}^{m}\left(C_{2m}^{m-k} + C_{2m}^{m+k}\right)\right) \\ &= 2^{-2m} \sum_{k=0}^{2m} C_{2m}^k = 1. \end{aligned} \tag{21}$$

Consider the second row of the matrix:

$$\begin{aligned} M_1 C &= \sum_{k=0}^{m} (-1)^k c_k \\ &= 2^{-2m}\left(C_{2m}^m + \sum_{k=1}^{m} 2(-1)^k C_{2m}^{m-k}\right) \\ &= 2^{-2m}\left(C_{2m}^m + \sum_{k=1}^{m} (-1)^k\left(C_{2m}^{m-k} + C_{2m}^{m+k}\right)\right) \\ &= 2^{-2m} \sum_{k=0}^{2m} (-1)^k C_{2m}^k \\ &= 0. \end{aligned} \tag{22}$$

Consider the third to $m + 1$ row of the matrix, $\forall r \in Z, 1 < r < m + 1$,

$$M_r C = 2^{1-2m} \sum_{k=1}^{m} (-1)^k C_{2m}^{m-k}\left(k^2\right)^{r-1}. \tag{23}$$

The validity of Theorem 5 can be established due to

$$\begin{aligned} &\sum_{k=1}^{m} (-1)^k C_{2m}^{m-k}\left(k^2\right)^{r-1} \\ &= \sum_{k=1}^{m} \frac{C_{2m}^{m-k} + C_{2m}^{m+k}}{2}(-1)^k\left(k^2\right)^{r-1} \\ &= 0 \times C_{2m}^m + \sum_{k=1}^{m} \frac{C_{2m}^{m-k} + C_{2m}^{m+k}}{2}(-1)^k\left(k^2\right)^{r-1} \\ &= \frac{1}{2} \sum_{k=0}^{2m} (-1)^k C_{2m}^k (m - k)^{2r-2}, \end{aligned} \tag{24}$$

and $(m - k)^{2r-2} = p(k)$is a $2r - 2$order polynomial to the variable$k$, which satisfies the conditions of Lemma 4 so $M_r C = 0$, since$M_0 C = 1$, $M_1 C = 0$, $M_r C = 0, r = 2, \ldots, m$, hence$MC = B$, the equation (16) has a unique solution and$MA = B$, $T_N^m(x) \equiv T_O^m(x)$, then$A = C$, and the rest of the Original Shannon-Cosine wavelet scale function and the Low-Complexity Shannon-Cosine wavelet scale function are equal, so Theorem 5 holds. □

Specific parameter values can be used to verify Theorem 5, and for the case when $m < 8$, the parameter values c_i are provided in Table 1. By comparing the values a_i in the literature [11], the two coefficients are found to be exactly equal.

4. Multiscale Shannon-Cosine Wavelet Interpolation Operator

In this section, a multiscale wavelet interpolation operator is constructed firstly based on the interpolation property of the Shannon-Cosine wavelet, which can be used to represent the smooth signal sparsely. Therefore, it can be used to solve time-fractal PDEs efficiently. Then, we analyze the time complexity of the interpolation operators constructed based on the two forms of the Shannon-Cosine wavelet, respectively.

4.1. Construction of the Multiscale Wavelet Interpolation Operation. The two forms of Shannon-Cosine wavelet and the Low-Complexity Shannon-Cosine wavelet function $S_O(x)$ and $S_N(x)$ have been introduced in Section 2, and the sequence of scale functions and the sequence of wavelet functions are, respectively, defined as

$$\begin{aligned} \phi_{j,k}(x) &= S_N\left(\frac{(x - x_n)}{\Delta}\right), \\ \varphi_{j,k}(x) &= \phi_{j+1,2k+1}(x), \end{aligned} \tag{25}$$

where $x_{j,n} = x_{\min} + nx_{\max} - x_{\min}/2^j, n = 0, 1, 2, \ldots, 2^j$, $\Delta = x_{\max} - x_{\min}/2^j, k = 0, 1, 2, \ldots, 2^j$.

Define the mapping s: $(j, k) \mapsto n$ as follows:

Table 1: Value of coefficient c_i in Low-Complexity Shannon-Cosine wavelet kernel function.

m	c_0	c_1	c_2	c_3	c_4	c_5	c_6	c_7
0	1							
1	1/2	1/2						
2	3/8	1/2	1/8					
3	5/16	15/32	3/16	1/32				
4	35/128	7/16	7/32	1/16	1/128			
5	63/256	105/256	15/64	45/512	5/256	1/512		
6	231/1024	99/256	495/2048	55/512	33/1024	3/512	1/2028	
7	429/2048	303/8192	1001/4096	1001/8192	91/2048	91/8192	7/4096	1/8192

$$s(j,k) = k2^{J-j} + 2^{J-j-1},$$
$$j_0 \le j < 2^J - 1, 0 \le k < 2^j - 1. \tag{26}$$

The inverse function of the function s in this paper is denoted by s^{-1}, when mod $(n, 2^{J-j_0}) = 0$, the definition of $s^{-1}(n)$ is complemented by $s^{-1}(n) = (j_0, n2^{J-j_0})$, and then there is a unique (j, k) corresponding to any integer $0 \le n \le 2^J$. We denote this mapping relationship by the following notation $= s_j^{-1}(n), k = s_k^{-1}(n)$.

The definition of $R_{i,m}^{j,j}$ is

$$R_{i,m}^{l,j} = \begin{cases} 1, & x_{l,i} = x_{j,m}, \\ 0, & \text{other}, \end{cases}$$

$$\mathbf{W}_0 = \begin{bmatrix} w_{s^{-1}(0)}(x_{J,0}) & w_{s^{-1}(1)}(x_{J,0}) & w_{s^{-1}(2)}(x_{J,0}) & \cdots & w_{s^{-1}(2^J)}(x_{J,0}) \\ w_{s^{-1}(0)}(x_{J,1}) & w_{s^{-1}(1)}(x_{J,1}) & w_{s^{-1}(2)}(x_{J,1}) & \cdots & w_{s^{-1}(2^J)}(x_{J,1}) \\ w_{s^{-1}(0)}(x_{J,2}) & w_{s^{-1}(1)}(x_{J,2}) & w_{s^{-1}(2)}(x_{J,2}) & \cdots & w_{s^{-1}(2^J)}(x_{J,2}) \\ \vdots & \vdots & \vdots & \vdots & \vdots \\ w_{s^{-1}(0)}(x_{J,2^J}) & w_{s^{-1}(1)}(x_{J,2^J}) & w_{s^{-1}(2)}(x_{J,2^J}) & \cdots & w_{s^{-1}(2^J)}(x_{J,2^J}) \end{bmatrix},$$

$$\mathbf{W}_1 = \begin{bmatrix} w'_{s^{-1}(0)}(x_{J,0}) & w'_{s^{-1}(1)}(x_{J,0}) & w'_{s^{-1}(2)}(x_{J,0}) & \cdots & w'_{s^{-1}(2^J)}(x_{J,0}) \\ w'_{s^{-1}(0)}(x_{J,1}) & w'_{s^{-1}(1)}(x_{J,1}) & w'_{s^{-1}(2)}(x_{J,1}) & \cdots & w'_{s^{-1}(2^J)}(x_{J,1}) \\ w'_{s^{-1}(0)}(x_{J,2}) & w'_{s^{-1}(1)}(x_{J,2}) & w'_{s^{-1}(2)}(x_{J,2}) & \cdots & w'_{s^{-1}(2^J)}(x_{J,2}) \\ \vdots & \vdots & \vdots & \vdots & \vdots \\ w'_{s^{-1}(0)}(x_{J,2^J}) & w'_{s^{-1}(1)}(x_{J,2^J}) & w'_{s^{-1}(2)}(x_{J,2^J}) & \cdots & w'_{s^{-1}(2^J)}(x_{J,2^J}) \end{bmatrix},$$

$$\mathbf{W}_2 = \begin{bmatrix} w''_{s^{-1}(0)}(x_{J,0}) & w''_{s^{-1}(1)}(x_{J,0}) & w''_{s^{-1}(2)}(x_{J,0}) & \cdots & w''_{s^{-1}(2^J)}(x_{J,0}) \\ w''_{s^{-1}(0)}(x_{J,1}) & w''_{s^{-1}(1)}(x_{J,1}) & w''_{s^{-1}(2)}(x_{J,1}) & \cdots & w''_{s^{-1}(2^J)}(x_{J,1}) \\ w''_{s^{-1}(0)}(x_{J,2}) & w''_{s^{-1}(1)}(x_{J,2}) & w''_{s^{-1}(2)}(x_{J,2}) & \cdots & w''_{s^{-1}(2^J)}(x_{J,2}) \\ \vdots & \vdots & \vdots & \vdots & \vdots \\ w''_{s^{-1}(0)}(x_{J,2^J}) & w''_{s^{-1}(1)}(x_{J,2^J}) & w''_{s^{-1}(2)}(x_{J,2^J}) & \cdots & w''_{s^{-1}(2^J)}(x_{J,2^J}) \end{bmatrix},$$

$$\mathbf{H} = \begin{bmatrix} H_{s_k^{-1}(0),0}^{s_j^{-1}(0),J} & H_{s_k^{-1}(0),1}^{s_j^{-1}(0),J} & H_{s_k^{-1}(0),2}^{s_j^{-1}(0),J} & \cdots & H_{s_k^{-1}(0),2^J}^{s_j^{-1}(0),J} \\ H_{s_k^{-1}(1),0}^{s_j^{-1}(1),J} & H_{s_k^{-1}(1),1}^{s_j^{-1}(1),J} & H_{s_k^{-1}(1),2}^{s_j^{-1}(1),J} & \cdots & H_{s_k^{-1}(1),2^J}^{s_j^{-1}(1),J} \\ H_{s_k^{-1}(2),0}^{s_j^{-1}(2),J} & H_{s_k^{-1}(2),1}^{s_j^{-1}(2),J} & H_{s_k^{-1}(2),2}^{s_j^{-1}(2),J} & \cdots & H_{s_k^{-1}(2),2^J}^{s_j^{-1}(2),J} \\ \vdots & \vdots & \vdots & \vdots & \vdots \\ H_{s_k^{-1}(2^J),0}^{s_j^{-1}(2^J),J} & H_{s_k^{-1}(2^J),1}^{s_j^{-1}(2^J),J} & H_{s_k^{-1}(2^J),2}^{s_j^{-1}(2^J),J} & \cdots & H_{s_k^{-1}(2^J),2^J}^{s_j^{-1}(2^J),J} \end{bmatrix},$$

$$H_{s_k^{-1}(m),n}^{s_j^{-1}(m),J} = \begin{cases} 1, & \text{mod}\left(n, 2^{J-j_0}\right) = 0, m = n, \\ 0, & \text{mod}\left(n, 2^{J-j_0}\right) = 0, m \ne n, \\ C_{s_k^{-1}(m),n}^{s_j^{-1}(m),J}, & \text{mod}\left(n, 2^{J-j_0}\right) \ne 0, \end{cases} \tag{27}$$

$$C_{k,n}^{j,J} = R_{2k+1,n}^{j+1,J} - \sum_{k_0=0}^{2^{j_0}} R_{k_0,n}^{j_0,J} \phi_{j_0,k_0}\left(x_{j+1,2k+1}\right) - \sum_{j_1=j_0}^{j-1} \sum_{k_1=0}^{2^{j_1-1}} C_{k_1,n}^{j_1,J} \varphi_{j_1,k_1}\left(x_{j+1,2k+1}\right),$$

$$w_{s^{-1}(n)}(x) = \begin{cases} \varphi_{s^{-1}(n)}(x), & \text{mod}\left(n, 2^{J-j_0}\right) \ne 0, \\ \phi_{s^{-1}(n)}(x), & \text{mod}\left(n, 2^{J-j_0}\right) = 0. \end{cases}$$

The data $F = [f(x_{J,0}), f(x_{J,1}), \ldots, f(x_{J,2^J})]^T$, along with its first-order derivative $D^1(F)$ and second-order derivative $D^2(F)$, can be represented in matrix format as follows:

$$\begin{aligned} F &= \mathbf{W}_0\mathbf{H}\mathbf{F}, \\ D^1(F) &= (\mathbf{W}_1)\mathbf{H}\mathbf{F}, \\ D^2(F) &= (\mathbf{W}_2)\mathbf{H}\mathbf{F}, \end{aligned} \tag{28}$$

where $\mathbf{W}_0, \mathbf{W}_1$, and $\mathbf{W}_2$ are defined as equation (34).

Let $f(x) \in L^2(\mathbb{R})$, which represents the space of measurable square-integrable functions. Then, the infinite series expansion of $f(x)$ with Shannon-Cosine wavelet converges uniformly to $f(x)$, i.e.,

$$f(x) = \sum_k b_k \phi_k(x) + \sum_{j\geq 0;k;} a_{j,k}\psi_{j,k}(x). \tag{29}$$

4.2. Fractional Population Diffusion Model. To compare and illustrate the advantages of the new Shannon-Cosine wavelet, we applied the multiscale Shannon-Cosine wavelet collocation method to obtain the numerical solutions of the time-fractional population diffusion model. The differences in key algorithms for implementing two Shannon-Cosine wavelets are first introduced and analyzed in terms of time complexity.

The Time-Fractional Population Diffusion Model (TFPDM) is a well-defined fractional partial differential equation (PDE) that highlights the spatial and temporal propagation of a virile gene in an infinite medium [19]. The TFPDM can be described as follows:

$$\begin{aligned} D_t^\alpha u(x,t) &= D_{xx}u(x,t) \\ &\quad + \lambda u(x,t)\left(1 - u^n(x,t)\right) + q(x,t). \end{aligned} \tag{30}$$

The initial and boundary conditions are

$$u(x,0) = f(x), u(0,t) = y_1(t), u(1,t) = y_2(t), \tag{31}$$

where $x \in R, 0 \leq x \leq 1, t > 0, 0 < \alpha \leq 1$, D_t^α denotes the Caputo [20] fractional derivative in time, and $y_1(t)$, $y_2(t)$, $f(x)$, and $q(x,t)$ are some known functions. The following specific TFPDM is considered for$\lambda = 1, n = 3$and

$$\begin{aligned} q(x,t) &= -2t - xt(t+x)\left(1 - t^3x^3(t+x)^3\right) \\ &\quad + \frac{x^2t^{1-\alpha}}{\Gamma(2-\alpha)} + \frac{2xt^{2-\alpha}}{\Gamma(3-\alpha)}, \end{aligned} \tag{32}$$

with the initial and boundary conditions$f(x) = 0$, $y_1(t) = 0$, $y_2(t) = t + t^2$, which has an exact solution [1]

$$u_{exa}(x,t) = xt^2 + tx^2. \tag{33}$$

The finite difference format [21] of the fractional order derivative part of equation (36) is given by

$$\begin{aligned} \frac{\partial^\alpha u(x,t_{n+1})}{\partial t^\alpha} &= \frac{\tau^{-\alpha}}{\Gamma(2-\alpha)}\sum_{k=0}^{n} b_k\left(u\left(x,t_{n+1-p}\right) - u\left(x,t_{n-k}\right)\right) \\ &\quad + O\left(\tau^{2-\alpha}\right), \end{aligned} \tag{34}$$

where $b_k = (k+1)^{1-\alpha} - k^{1-\alpha}$, Using the wavelet allocation method, the differential form of the right-hand side of equation (36) is obtained. Moreover, the nonlinear term is linearized by the method introduced by Rubin and Graves [22]. The resulting expressions are as follows:

$$\begin{aligned} \frac{\partial^2 u}{\partial x^2} + u\Big|_{(x_i,t_{n+1})} &= u_{xx} + u_j(x_m,t_{n+1}), \\ \left(u^4\right)\Big|_{(x_i,t_{n+1})} &= 4\left(u_i^n\right)^3 u_i^{n+1} - 3\left(u_i^n\right)^4 + O(\tau)^2. \end{aligned} \tag{35}$$

Bringing the difference form to the equation (36), ignoring the infinitesimal terms gives the finite difference form of the equation.

$$\begin{aligned} &\frac{\tau^{-\alpha}}{\Gamma(2-\alpha)}\sum_{k=0}^{n} b_k\left(u\left(x_i,t_{n+1-p}\right) - u\left(x_i,t_{n-k}\right)\right) \\ &= u_{xx} + u_i^{n+1} - 4\left(u_i^n\right)^3 u_i^{n+1} + 3\left(u_i^n\right)^4 \\ &\quad + q\left(x_i,t_{n+1}\right). \end{aligned} \tag{36}$$

The solution of the general iterative method of TFPDM in matrix form is given by

$$\begin{aligned} &4r\left(V_j^n\right)^3 V_j^{n+1} + (1-r)V_j^{n+1} - r\left(V^{''}\right)_j^{n+1} \\ &= b_n V_j^0 + 3r\left(V_j^n\right)^4 + \sum_{p=0}^{n-1}\left(b_p - b_{p+1}\right)V_j^{n-p} \\ &\quad + rQ^{n+1}. \end{aligned} \tag{37}$$

The boundary conditions generate other equations for $u_j(x_0,t_n)$ and $u_j(x_{2^j},t_n)$:

$$\begin{aligned} u_j(x_0,t_{n+1}) &= y_1(t_{n+1}), \\ u_j(x_{2^j},t_{n+1}) &= y_2(t_{n+1}). \end{aligned} \tag{38}$$

Let

$$\begin{aligned} r &= \tau^\alpha\Gamma(2-\alpha), F = \mathrm{diag}\left(4r\left(V_j^n\right)^3\right), \\ V_j^n &= \left(u_j(x_0,t_n), u_j(x_1,t_n), \ldots, u_j(x_{2^j},t_n)\right)^T, \\ Q^n &= \left(q(x_0,t_n), q(x_1,t_n), \ldots, q(x_{2^j},t_n)\right)^T. \end{aligned} \tag{39}$$

The matrix form of the equation (36) based on the multiscale wavelet allocation method [23] is

(1) Initialize: Given $V_j^0, n = 0$
(2) **while** $n < N$ **do**
(3) Compute $\mathbf{A^{n+1}}\ B^{n+1}$
(4) Solve $\mathbf{A^{n+1}} V_j^{n+1} = B^{n+1}$
(5) Update V_j^n with V_j^{n+1}
(6) $n = n + 1$
(7) **end while**

Algorithm 1: Wavelet-based iterative solver.

Table 2: Relative numerical error of Shannon-Cosine wavelet spectral method to approximate the solution of the TFPDM at $t = 0.1$ with $m = 3, \tau = 4e - 5\ J = 7, j_0 = 6$ for different N and α.

N	$\alpha = 0.2$	$\alpha = 0.4$	$\alpha = 0.6$	$\alpha = 0.8$
7	1.6479$e-01$	1.6480$e-01$	1.6515$e-01$	1.6597$e-01$
7.43733035	1.3534$e-01$	1.1386$e-01$	8.6807$e-02$	5.8179$e-02$
8	3.4742$e-01$	3.4265$e-01$	3.3926$e-01$	3.3951$e-01$
11	1.8052$e-01$	1.5812$e-01$	1.3251$e-01$	1.1110$e-01$
11.26119977	1.7245$e-01$	1.4466$e-01$	1.0889$e-01$	6.8392$e-02$
12	1.7906$e-01$	1.5166$e-01$	1.1687$e-01$	7.8928$e-02$

$$\begin{aligned}&(F + (1-r)\mathbf{I} - r\mathbf{W}_2)V_j^{n+1}\\ &= b_n V_j^0 + 3r\left(V_j^n\right)^4 + rQ^{n+1}\\ &\quad + \sum_{k=0}^{n-1}(b_k - b_{k+1})V_j^{n-k},\end{aligned} \tag{40}$$

and where $\mathbf{W}_2$ is defined by equation (34), both $\varphi_{s^{-1}(n)}(x)$ and $\phi_{s^{-1}(n)}(x)$ within that formula refer either to the Shannon-Gabor wavelet function [24] or the Shannon-Cosine wavelet function.

The solution to equation (40) is given by

$$V^{n+1} = \left(\mathbf{A^{n+1}}\right)^{-1} B^{n+1}, \tag{41}$$

where

$$\begin{aligned}A^{n+1} &= (F + (1-r)\mathbf{I} - r\mathbf{W}_2)\\ B^{n+1} &= b_n V_j^0 + 3r\left(V_j^n\right)^4 + rQ^{n+1}\\ &\quad + \sum_{k=0}^{n-1}(b_k - b_{k+1})V_j^{n-k}.\end{aligned} \tag{42}$$

The calculation of the relative numerical error is given by

$$e = \frac{1}{2^j + 1}\sqrt{\sum_{i=0}^{2^j}\left(u_{\text{num}}(x_i, t) - u_{\text{exa}}(x_i, t)\right)^2}. \tag{43}$$

We use a combination of the multiscale Shannon-Cosine wavelet spectral method and iteration technique for the numerical solution of equations (30) and (40) compared to Shannon–Gabor [24] wavelet.

The core idea of this algorithm is to iteratively solve the linear system by updating the matrix A and vector B at each step, using the wavelet-based method to approximate the solution. The algorithm successively refines the solution until convergence is achieved. The specific process is shown in Algorithm 1.

Table 2 presents the average error of the TFPDM approximate solution at $t = 0.1$ using the Shannon-Cosine wavelet spectral method, with parameters $m = 3, \tau = 4e - 5$, $J = 7, j_0 = 6$ for varying values of N and α. This indicates that the Shannon-Cosine wavelet spectral method offers an approximation for TFPDM that is closely aligned with the exact solution. Furthermore, the numerical error is notably smaller for specific values that meet the normalization condition compared to those that round towards negative or positive infinity.

Table 3 displays a comparison of error among two wavelet spectral methods to approximate the solution of the TFPDM, which demonstrates that the multiscale Shannon-Cosine wavelet spectral method has better numerical stability compared to Shannon–Gabor wavelet. The figure shown in Figure2 displays the numerical solution with parameters $\alpha = 0.4, J = 7$, $j_0 = 0$, eps $= 4e - 5$, $m = 3$, and $N = 15.18988168$.

Figure 3 displays the numerical solutions and relative numerical errors when using the multiscale Shannon-Cosine wavelet spectral methods for the TFPDM, across different α values. The parameters adopted in this analysis are $m = 3$, $\tau = 4e - 4$, $J = 7$, and $j_0 = 6$. The findings reinforce the superior numerical stability provided by the multiscale Shannon-Cosine wavelet spectral method under these conditions.

Figure 2 illustrates the numerical solutions using the multiscale Shannon-Cosine wavelet spectral methods to approximate the solution of TFPDM for different values of x, when the time $t = 0.02, 0.04, 0.06, 0.08, 0.10$. The comparison shows that the multiscale Shannon-Cosine wavelet spectral method displays superior numerical stability.

According to the analysis of experimental results, an increase in the scale parameter j is positively correlated with a decrease in experimental error. This indicates that increasing j can improve the stability and consistency of the experiment. Similarly, an increase in the fractional-order

Table 3: Comparison of relative numerical error among two methods to approximate the solution of the TFPDM at $t = 0.1$ with $m = 3, \tau = 4e-5, r = 3.2, J = j, j_0 = 0, N = 63.04503351$.

α	j	Shannon–Gabor wavelet	Shannon-Cosine wavelet
0.2	6	$1.8343e-02$	$1.4200e-02$
	7	$9.7604e-03$	$6.9733e-03$
	8	$5.0813e-03$	$3.0169e-03$
0.4	6	$1.7916e-02$	$1.3815e-02$
	7	$9.6249e-03$	$6.8486e-03$
	8	$5.0398e-03$	$2.9763e-03$
0.6	6	$1.7360e-02$	$1.3318e-02$
	7	$9.4492e-03$	$6.6877e-03$
	8	$4.9865e-03$	$2.9244e-03$
0.8	6	$1.6699e-02$	$1.2732e-02$
	7	$9.2445e-03$	$6.5028e-03$
	8	$4.9278e-03$	$2.8689e-03$

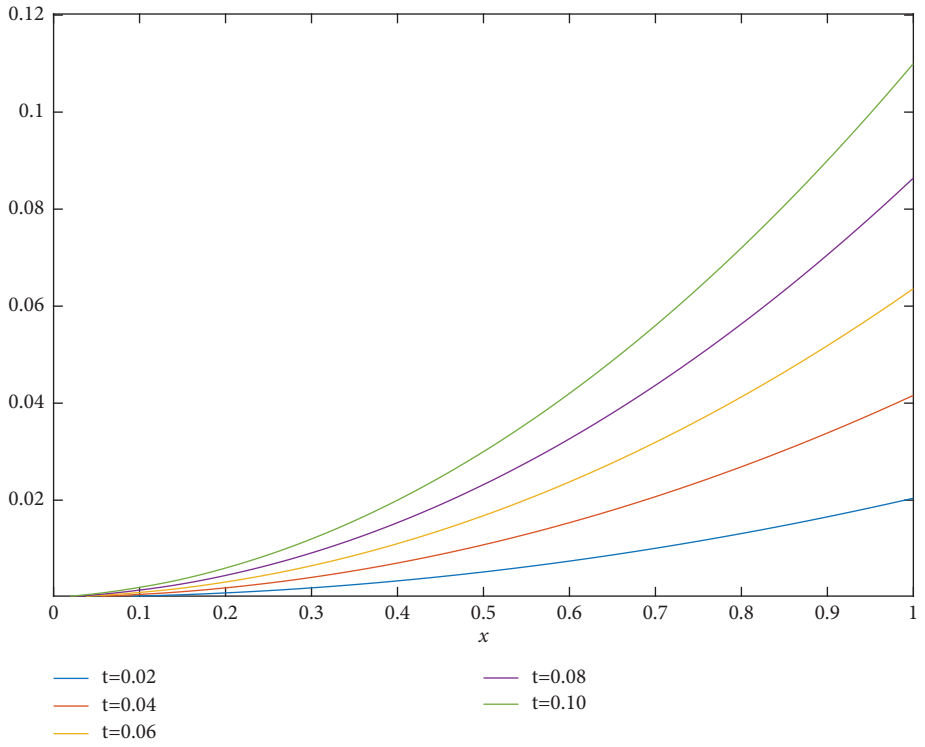

Figure 2: Numerical solution of TFPDM at $t = 0.1$.

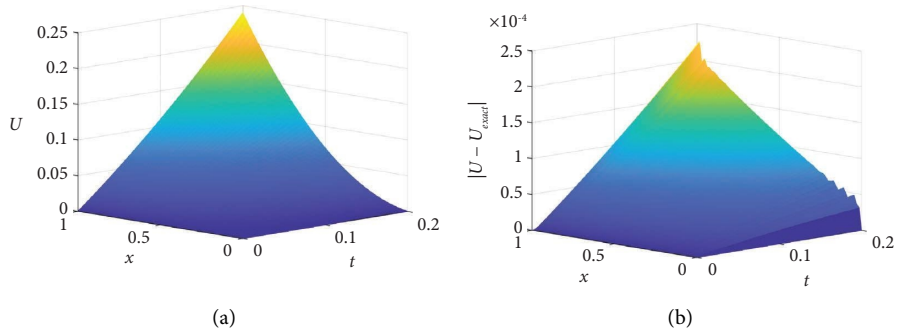

(a) (b)

Figure 3: Continued.

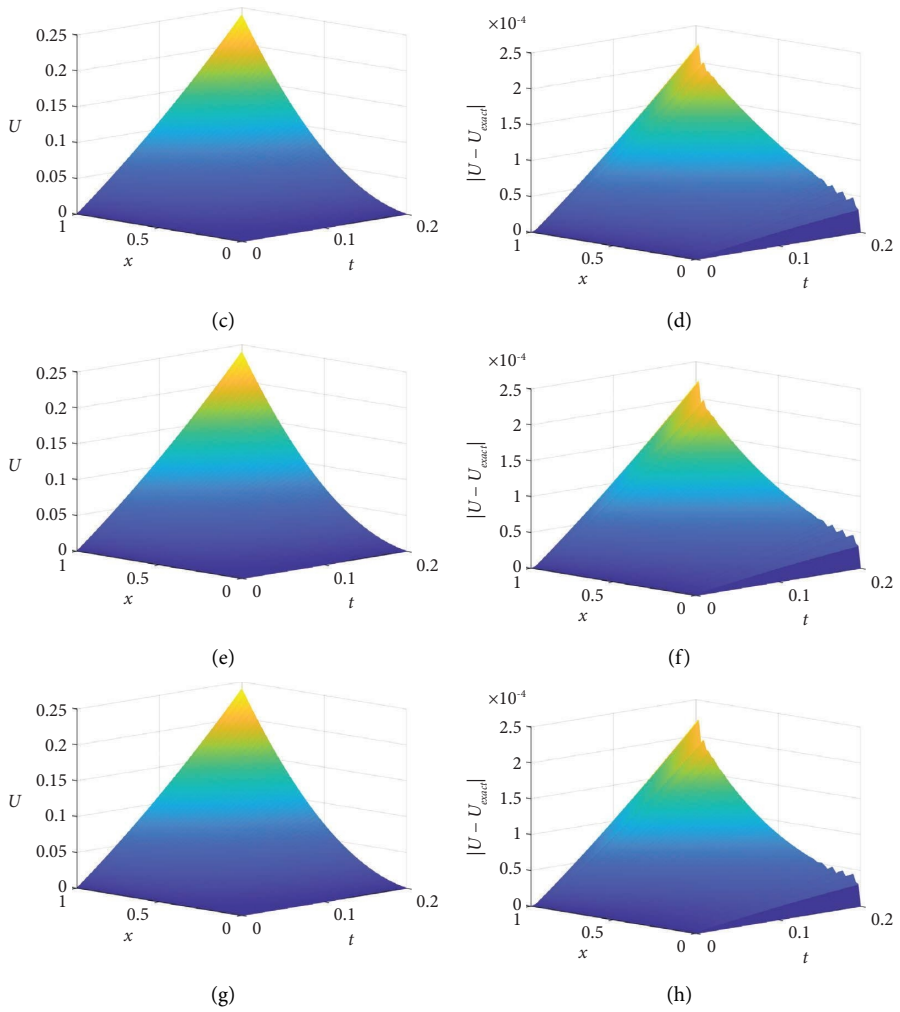

FIGURE 3: Numerical solution and relative numerical error of TFPDM at $t \in [0, 0.2]$. (a) Numerical solution at $\alpha = 0.2$. (b) Relative numerical error at $\alpha = 0.2$. (c) Numerical solution at $\alpha = 0.4$. (d) Relative numerical error at $\alpha = 0.4$. (e) Numerical solution at $\alpha = 0.6$. (f) Relative numerical error at $\alpha = 0.6$. (g) Numerical solution at $\alpha = 0.8$. (h) Relative numerical error at $\alpha = 0.8$.

exponent parameter α also leads to a reduction in experimental error, potentially reducing error sources and enhancing experimental accuracy. However, the increase in the time variable t is positively associated with an increase in experimental error, possibly due to system or condition variations. In summary, the scale parameter j and the fractional-order exponent parameter α have a positive impact on reducing experimental error, while the increase in the time variable t is linked to error increase. These findings provide valuable insights into the reliability and accuracy of the experimental results.

5. Conclusion

In this paper, we present the Low-Complexity Shannon-Cosine wavelet by substituting the Original Shannon-Cosine with the positive and even power of the cosine function. It has been rigorously demonstrated that the Low-Complexity Shannon-Cosine wavelet is equivalent to the Original Shannon-Cosine wavelet via trigonometric series, utilizing the pertinent properties of combinatorial numbers.

The primary advantage of the Low-Complexity Shannon-Cosine wavelet lies in the elimination of certain parameter calculations present in the earlier version, thereby enhancing the efficiency of programming. Numerical experiments have established that the Shannon-Cosine wavelet serves as an invaluable technique for achieving high-precision numerical solutions to various fractional-order partial differential equation problems in engineering applications.

Data Availability

No underlying data were collected or produced in this study.

Conflicts of Interest

The authors declare that they have no conflicts of interest.

Acknowledgments

This study was supported by the National Natural Science Foundation of China (grant no. 61871380), Beijing Natural Science Foundation (grant no. 4172034), Shandong Provincial

Natural Science Foundation (grant no. ZR2020MF019), and Beijing Innovation Consortium of Agriculture Research System (BAIC11-2023).

References

[1] G. Ahmadnezhad, N. Aghazadeh, and S. Rezapour, "Haar wavelet iteration method for solving time fractional Fisher's equation," *Computational Methods for Differential Equations*, vol. 8, no. 3, pp. 505–522, 2020.

[2] T. Eriqat, M. A N. Oqielat, Z. Al-Zhour, A. El-Ajou, and A. S. Bataineh, "Revisited Fisher's equation and logistic system model: a new fractional approach and some modifications," *International Journal of Dynamics and Control*, vol. 11, no. 2, pp. 555–563, 2023.

[3] T. Sardar, S. Rana, and J. Chattopadhyay, "A mathematical model of dengue transmission with memory," *Communications in Nonlinear Science and Numerical Simulation*, vol. 22, no. 1-3, pp. 511–525, 2015.

[4] X. Zhang and J. Liu, "An analytic study on time-fractional Fisher equation using homotopy perturbation method," *Walailak Journal of Science and Technology*, vol. 11, no. 11, pp. 975–985, 2014.

[5] M. M. Al Qurashi, Z. Korpinar, D. Baleanu, and M. Inc, "A new iterative algorithm on the time-fractional Fisher equation: residual power series method," *Advances in Mechanical Engineering*, vol. 9, no. 9, Article ID 168781401771600, 2017.

[6] C. Cattani, "Fractional calculus and shannon wavelet," *Mathematical Problems in Engineering*, vol. 2012, Article ID 502812, 26 pages, 2012.

[7] H. Rabbouch and F. Saadaoui, "A wavelet-assisted subband denoising for tomographic image reconstruction," *Journal of Visual Communication and Image Representation*, vol. 55, pp. 115–130, 2018.

[8] M. Liu, S. Mei, P. Liu, Y. Gasimov, and C. Cattani, "A new x-ray medical-image-enhancement method based on multiscale shannon–cosine wavelet," *Entropy*, vol. 24, no. 12, p. 1754, 2022.

[9] I. Daubechies and C. Heil, "Ten lectures on wavelets," *Computers in Physics*, vol. 6, no. 6, p. 697, 1992.

[10] C. Cattani, "Harmonic wavelets towards the solution of nonlinear pde," *Computers & Mathematics with Applications*, vol. 50, no. 8-9, pp. 1191–1210, 2005.

[11] S. Mei and W. Gao, "Shannon–cosine wavelet spectral method for solving fractional fokker–planck equations," *International Journal of Wavelets, Multiresolution and Information Processing*, vol. 16, no. 3, Article ID 1850021, 2018.

[12] H. Wang, X. Zhang, and S. Mei, "Shannon-cosine wavelet precise integration method for locust slice image mixed denoising," *Mathematical Problems in Engineering*, vol. 2020, Article ID 4989735, 17 pages, 2020.

[13] H. Wang, J. Liu, L. Liu, M. Zhao, and S. Mei, "Coupling technology of opensurf and shannon-cosine wavelet interpolation for locust slice images inpainting," *Computers and Electronics in Agriculture*, vol. 198, Article ID 107110, 2022.

[14] A. Wang, L. Li, S. Mei, and K. Meng, "Hermite interpolation based interval shannon-cosine wavelet and its application in sparse representation of curve," *Mathematics*, vol. 9, no. 1, p. 1, 2020.

[15] W. Haonian, Y. Li, T. Yuyuan, and N. Xiangfan, "Method improving low signal-to-noise ratio of velocity test signals for laser-induced shock waves," *Optics & Laser Technology*, vol. 155, Article ID 108362, 2022.

[16] C.-S. Huang, J. G. O'Hara, and S. Mataramvura, "Highly efficient shannon wavelet-based pricing of power options under the double exponential jump framework with stochastic jump intensity and volatility," *Applied Mathematics and Computation*, vol. 414, Article ID 126669, 2022.

[17] S. L. Mei, H.-L. Lv, and Q. Ma, "Construction of interval wavelet based on restricted variational principle and its application for solving differential equations," *Mathematical Problems in Engineering*, vol. 2008, Article ID 629253, 14 pages, 2008.

[18] J. Shi, *Combinatorial Identities*, Press of University of Science and Technology of China, Hefei, China, 1989.

[19] A. Demir, M. A. Bayrak, and E. Ozbilge, "An approximate solution of the time-fractional Fisher equation with small delay by residual power series method," *Mathematical Problems in Engineering*, vol. 2018, Article ID 9471910, 8 pages, 2018.

[20] T. Abdeljawad, "On riemann and caputo fractional differences," *Computers & Mathematics with Applications*, vol. 62, no. 3, pp. 1602–1611, 2011.

[21] R. Gorenflo and F. Mainardi, *Fractional Calculus*, Springer, Berlin, Germany, 1997.

[22] S. G. Rubin and R. A. Graves Jr, "A cubic spline approximation for problems in fluid mechanics," Nasa Technical Report, NASA, Washington, DC, USA, 1975.

[23] T. Akram, M. Abbas, and A. Ali, "A numerical study on time fractional Fisher equation using an extended cubic b-spline approximation," *The Journal of Mathematics and Computer Science*, vol. 22, no. 2, pp. 85–96, 2020.

[24] D. K. Hoffman, G. W. Wei, D. S. Zhang, and D. J. Kouri, "Shannon–gabor wavelet distributed approximating functional," *Chemical Physics Letters*, vol. 287, no. 1-2, pp. 119–124, 1998.